Energy Balance and Time Dependence of a Magnetotail Electron Diffusion Region

D.S. Payne[1], K.J. Genestreti[2], K. Germaschewski[1], M.R. Argall[1], R.B. Torbert[1], I. Dors[1], A. Ardakani[1]

[1]University of New Hampshire, Durham, NH, USA
[2]Southwest Research Institute, Durham, NH, USA

Key Points:

- Poynting's theorem terms are evaluated for an MMS observed magnetotail electron diffusion region (EDR)
- The assumption of quasi two dimensional reconnection improves the balance of the terms in Poynting's theorem
- The time evolution in Poynting's theorem is negligible, however large timescale evolution of the EDR cannot be ruled out

Corresponding author: Dominic Payne, dsp1007@wildcats.unh.edu

Abstract

We examine the July 11th, 2017 electron diffusion region (EDR) observed by the Magnetospheric Multiscale (MMS) mission using Poynting's theorem. The terms in Poynting's theorem are determined using a linear gradient approximation to obtain barycentric averages within the MMS tetrahedron. We find that Poynting's theorem is approximately balanced in the EDR, and the balance is improved if the calculation of $\boldsymbol{\nabla} \cdot \vec{S}$ is restricted to the LN plane. The work rate per unit volume $\vec{J} \cdot \vec{E}$ is mostly balanced by the divergence of the electromagnetic energy flux $\boldsymbol{\nabla} \cdot \vec{S}$, indicating that the electromagnetic energy density remains relatively constant within the EDR during the encounter. We also use particle-in-cell (PIC) simulations to examine Poynting's theorem near an x-line evolving in time. The central EDR in the simulation is characterized by approximate time independent balance in Poynting's theorem during reconnection growth, while the outer EDR exhibits time-dependent fluctuations indicative of more chaotic behavior.

1 Introduction

Magnetic reconnection is a process that occurs in magnetized plasmas, where magnetic fields with antiparallel components converge and merge, resulting in a topological transformation of the magnetic field and an energized plasma population. In these regions, such at the boundary of Earth's magnetopause or in the magnetotail, some portion of the inflowing magnetic energy is converted into kinetic and thermal energy in the plasma. This conversion of energy is often intermittent, but it can also be quasi-steady and even continuous over the course of hours (Frey et al., 2003). The energy conversion rate per unit volume is given by $\vec{J} \cdot \vec{E}$, where $\vec{J}$ is the current density and $\vec{E}$ is the electric field. Often in reconnection studies, the energy conversion rate in the electron rest frame is of greater interest, because it is a measure of the work done to the plasma by the non-ideal electric field, which is of great importance to understanding the fundamental processes that underlie reconnection (Zenitani et al., 2011). This term is given by $\vec{J} \cdot \vec{E}' = \vec{J} \cdot (\vec{E} + \vec{v_e} \times \vec{B})$, where $\vec{v_e}$ and $\vec{B}$ are the electron velocity and the magnetic field, respectively. $\vec{J} \cdot \vec{E}'$ is concentrated around the electron diffusion region (EDR) and separatrices, where frozen-in electrons become decoupled from the magnetic fields (Burch & Phan, 2016). For this reason, $\vec{J} \cdot \vec{E}'$ is often used as an identifier for the EDR in multi-spacecraft studies of reconnection (Burch & Phan, 2016; Torbert et al., 2018; Zenitani

et al., 2011). To examine energy balance at the EDR, we use the general expression $\vec{J}\cdot\vec{E}$ here, since it is not in the plasma rest frame and is more relevant to energy budget considerations.

Within a region where energy conversion occurs (where $\vec{J}\cdot\vec{E} > 0$), the net loss of electromagnetic energy corresponds to a decrease in the electromagnetic energy density and/or electromagnetic energy flux into the region. This formulation of the conservation of energy is Poynting's theorem, given by

$$\frac{\partial u}{\partial t} = -\boldsymbol{\nabla}\cdot\vec{S} - \vec{J}\cdot\vec{E} \tag{1}$$

where u is the electromagnetic energy density and $\vec{S}$ is the electromagnetic energy flux, or Poynting flux. It is important to understand the relative magnitudes of each term at different locations on the x-line and different times during its evolution, because it describes how and where on the x-line electromagnetic energy density is lost (or gained). Having a better understanding of the dynamics of energy may be useful in describing the physics of reconnection growth and the conditions that cause reconnection to be steady or time varying. In the time-independent case, where $\frac{\partial u}{\partial t} = 0$, the net loss or gain of electromagnetic energy must be balanced by the net gain or loss of plasma energy respectively, which can come in various forms such as heating or bulk plasma acceleration.

The terms in equation 1 have been previously studied in the context of energy release and conversion during reconnection using particle-in-cell (PIC) and magnetohydrodynamic (MHD) simulations (Birn & Hesse, 2005, 2010). These studies investigated $\vec{J}\cdot\vec{E}$ and the divergence of various energy fluxes, including Poynting flux, near the EDR. K. J. Genestreti et al. (2018) used MMS to evaluate in-situ measurements of the terms in equation 1 for an EDR encounter at the magnetopause. They found that the left and right hand sides of equation 1 balanced reasonably well, to within approximately 50% uncertainty. Overall, the event was strongly time dependent($\frac{\partial u}{\partial t} \neq 0$)near the x-line, due to imbalance between $\vec{J}\cdot\vec{E}$ and $\boldsymbol{\nabla}\cdot\vec{S}$ terms. The exception was at the current sheet center, where equation 1 exhibited time-independence ($\frac{\partial u}{\partial t} = 0$).

Here we present an evaluation of Poynting's theorem during the July 11th, 2017 EDR encounter(Torbert et al., 2018). In section 2, we discuss the tools used in this study and the methods used to calculate the terms in equation 1. In section 3 we include an overview of the event and our in-situ results, an analysis of the term $\boldsymbol{\nabla}\cdot S$ in the results, and a reconstruction of $\boldsymbol{\nabla}\cdot S$ to compare. In section 4, we present results from

a PIC simulation, where we evaluate the terms in equation 1 in the EDR and their evolution over time. In section 5 we summarize the results and discuss their implications.

We find that there is very little time evolution of u in the central EDR on July 11th, indicating that the EDR is not evolving on rapid electron timescales. However, we also find that time evolution of u in a 2D PIC simulation is negligible compared to the other terms in Poynting's theorem throughout the growth phase of reconnection, which suggests that ion timescale evolution could still be an important factor.

2 Data and Methods

2.1 Instrumentation

This study makes use of high time resolution burst mode data from the suite of particle and field instruments aboard MMS. Magnetic field data comes from the fluxgate magnetometers (FGM), which measure DC magnetic field vectors at 128 samples per second (Russell et al., 2016). Electric field data comes from the electric field double probes (EDP), which measure spin plane (Lindqvist et al., 2016) and axial (Ergun et al., 2016) components of the electric field at 8,196 samples per second. Particle data comes from the electron and ion spectrometers part of the fast plasma investigation (FPI) (Pollock et al., 2016). Level 2 (L2) data is used for all the field and plasma quantities except for the electric fields, where we use better calibrated L3 electric field data for the July 11th event.

2.2 Simulation

This study includes a 2D PIC simulation with an initial Harris current sheet configuration using the plasma simulation code (PSC) described in Germaschewski et al. (2016). The domain size is $L_x \times L_z = 80d_i \times 20d_i$ with an ion to electron mass ratio of $\frac{m_i}{m_e} = 100$, 300 particles per cell (ppc), ion to electron temperature ratio $\frac{T_i}{T_e} = 5$, and a background current sheet density to initial density ratio of $\frac{n_b}{n_0} = 0.05$.

2.3 Method

The tetrahedron formed by the MMS spacecraft provides a volume within which the quantities in equation 1 can be determined. The divergence of Poynting flux is a barycen-

tric value obtained using a linear gradient approximation (Paschmann & Schwartz, 2000), so the other terms are also expressed as barycentric averages to remain consistent.

$$\frac{\partial \langle u \rangle}{\partial t} = -\boldsymbol{\nabla} \cdot \vec{S} - \langle \vec{J} \rangle \cdot \langle \vec{E} \rangle \tag{2}$$

Poynting's theorem describes the spatial and temporal variation of electromagnetic energy density, so the relationship between terms in equation 1 is frame dependent. We are interested in the relative values of the terms in Poynting's theorem at an x-line, therefore the terms are determined in the x-line frame. This can be done using the velocity of the x-line ($\vec{v}_{xl}$) determined by four-spacecraft timing analysis of the B_z reversal. With this velocity, we can express the total convective derivative of the energy density

$$\frac{du}{dt} = \left.\frac{\partial u}{\partial t}\right|_{xl} + \vec{v}_{xl} \cdot \nabla u \tag{3}$$

This breaks the $\frac{du}{dt}$ observed by MMS into a purely temporal term and a spatial term associated with the motion of the x-line relative to MMS. Therefore, to obtain $\left.\frac{\partial u}{\partial t}\right|_{xl}$ the spatial term in the convective derivative must be subtracted from the $\frac{du}{dt}$ measured by MMS

$$\left.\frac{\partial u}{\partial t}\right|_{xl} = \frac{du}{dt} - \vec{v}_{xl} \cdot \nabla u \tag{4}$$

For the remainder of this paper, $\frac{\partial u}{\partial t}$ for the July 11th EDR will be in the x-line frame according to equation 4. The residual of the calculation will be any imbalance in the left and right hand sides of equation 2 ($\frac{\partial u}{\partial t} + \boldsymbol{\nabla} \cdot \vec{S} + \vec{J} \cdot \vec{E} \neq 0$)

To evaluate the terms in equation 1 in the PIC simulation, we compute a 2D $\boldsymbol{\nabla} \cdot \vec{S}$ along L and N, as there are no spatial derivatives along M in the simulation. $\vec{J} \cdot \vec{E}$, however, includes contributions along L, M and N. To evaluate all three terms in equation 1 at the same timestep, we calculate $\frac{\partial u}{\partial t}$ directly from $\vec{J} \cdot \vec{E}$ and the 2D $\boldsymbol{\nabla} \cdot \vec{S}$ according to equation 1, ensuring that the residual of the calculation is zero.

3 Energy Balance in the July 11th EDR

3.1 Event Overview

On July 11th, 2017, MMS encountered an EDR about 22 Earth radii into the magnetotail at approximately 22:34 UT (Torbert et al., 2018). MMS observed multiple signatures of reconnection, such as reversals in both B_L and B_N, Hall E_N components, and

a flow reversal in v_{eL} (figure 1). The spacecraft separation was roughly 15 km, and within the width of the current sheet. The trajectory was largely along the L axis of the x-line, and remained close to current sheet during the encounter as indicated by the small B_L.

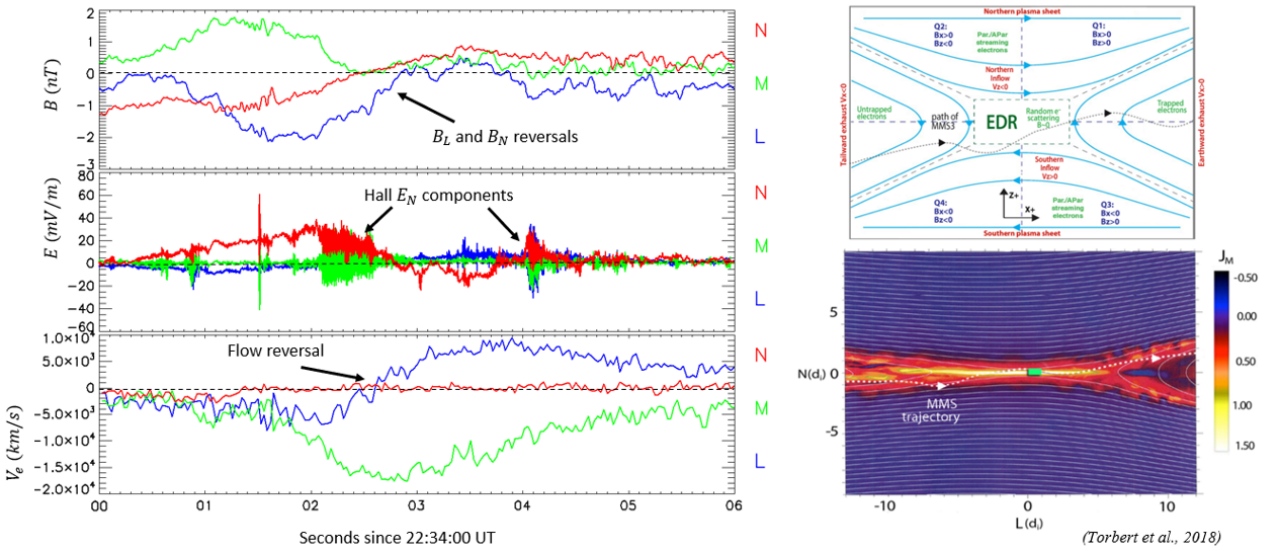

Figure 1. Overview of the July 11th EDR encounter. Left: magnetic field, electric field, and electron bulk velocity from MMS3. Right: MMS path through the EDR (diagram and simulation) from Torbert et al. (2018)

The July 11th EDR has been studied extensively, and has been compared to a simulation with similar parameters to determine the reconnection rate and the reconnection electric field(T. Nakamura et al., 2018; Torbert et al., 2018; Genestreti et al., 2018). The EDR exhibited evidence of laminar particle acceleration and quasi-2D force balance (R. Nakamura et al., 2019; Egedal et al., 2019).

3.2 Poynting's Theorem in the EDR

The initial results of our Poynting's theorem calculations in the frame of the X-line are shown in figure 2a. There is a close balance between the energy transfer rate and the divergence of the electromagnetic energy flux, where $-\langle\vec{J}\rangle \cdot \langle\vec{E}\rangle$ is roughly equivalent to $\boldsymbol{\nabla}\cdot\vec{S}$, and therefore $\frac{\partial\langle u\rangle}{\partial t}$ is close to zero, meaning that the reconnection is relatively

steady state. Despite this, there is still a discrepancy betweeen $-\langle\vec{J}\rangle \cdot \langle\vec{E}\rangle$ and $\boldsymbol{\nabla} \cdot \vec{S}$ from 22:34:02-03 UT that is not completely accounted for by a change in $\frac{\partial\langle u\rangle}{\partial t}$.

To investigate this discrepancy further, we calculate a divergence term by defining a 'moments' $(\boldsymbol{\nabla} \cdot \vec{S})_{mom}$, for each spacecraft, given by

$$(\boldsymbol{\nabla} \cdot \vec{S})_{mom} = -\frac{\partial u}{\partial t} - \vec{J} \cdot \vec{E} \tag{5}$$

where u, J, and E are all determined from one spacecraft. $\frac{\partial u}{\partial t}$ for each spacecraft is still calculated in the x-line frame by subtracting $\vec{v}_{xl} \cdot \nabla u$ from each $\frac{du}{dt}$ (equation 4), using the same $\vec{v}_{xl}$ and ∇u. Equation 5 gives a value for the divergence of Poynting flux at each corner of the MMS tetrahedron that balances Poynting's theorem at those points. These are plotted for each of the MMS spacecraft in figure 2b. There is a discrepancy between their average, $\left\langle(\boldsymbol{\nabla} \cdot \vec{S})_{mom}\right\rangle$, and the original barycentric calculation of $\boldsymbol{\nabla} \cdot \vec{S}$ (figure 2c). The close agreement between the four spacecraft suggest that they were all in a similar region, therefore the larger than expected $\boldsymbol{\nabla} \cdot \vec{S}$ therefore does not appear to be due to any significant difference from one spacecraft. The next step taken was to break the calculation of $\boldsymbol{\nabla} \cdot \vec{S}$ down into its individual components to look into any issues that may be causing the imbalance in Poynting's theorem.

In figure 2d, we show the components whose sum make up $\boldsymbol{\nabla} \cdot \vec{S}$, where

$$\boldsymbol{\nabla} \cdot \vec{S} = \frac{\partial S_L}{\partial L} + \frac{\partial S_M}{\partial M} + \frac{\partial S_N}{\partial N} \tag{6}$$

The LMN coordinate system can be expressed in GSE coordinates as L = [0.948, -0.255, -0.189], M = [0.182, 0.925, -0.335], N = [0.260, 0.283, 0.923] (Genestreti et al., 2018).

As expected for quasi-2D reconnection, the fields in the diverging reconnection outflow produce a positive $\frac{\partial S_L}{\partial L}$, and the converging inflowing fields produce a negative $\frac{\partial S_N}{\partial N}$. What is unexpected in figure 2d is the large negative $\frac{\partial S_M}{\partial M}$, which would indicate that fields are converging to the x point along both the N and M axes to a similar degree. Also note that the $\frac{\partial S_M}{\partial M}$ component has a large spike at 22:34:02 UT which also can be seen in $\boldsymbol{\nabla} \cdot \vec{S}$ in figure 2. There can be some component $\vec{S}$ along M, but there should be near zero gradient along M for quasi-2D reconnection. This large contribution to $\boldsymbol{\nabla} \cdot \vec{S}$ along the M direction is likely the biggest contributor to the imbalance in $\boldsymbol{\nabla} \cdot \vec{S}$ and Poynting's theorem.

To check if this is the case, we test whether the assumption of quasi-2D reconnection improves the balance of Poynting's theorem by eliminating $\frac{\partial S_M}{\partial M}$ from the divergence

156 calculation. By assuming 2D reconnection and eliminating $\frac{\partial S_M}{\partial M}$ contributions, Poynt-
157 ing's theorem is closer to being balanced overall (figure 2e), however this does contribute
158 to more imbalance from 22:34:01-02 UT. The residual is comparable in magnitude to the
159 results in K. J. Genestreti et al. (2018). For the remaining sections of this paper we make
the quasi-2D assumption for this event.

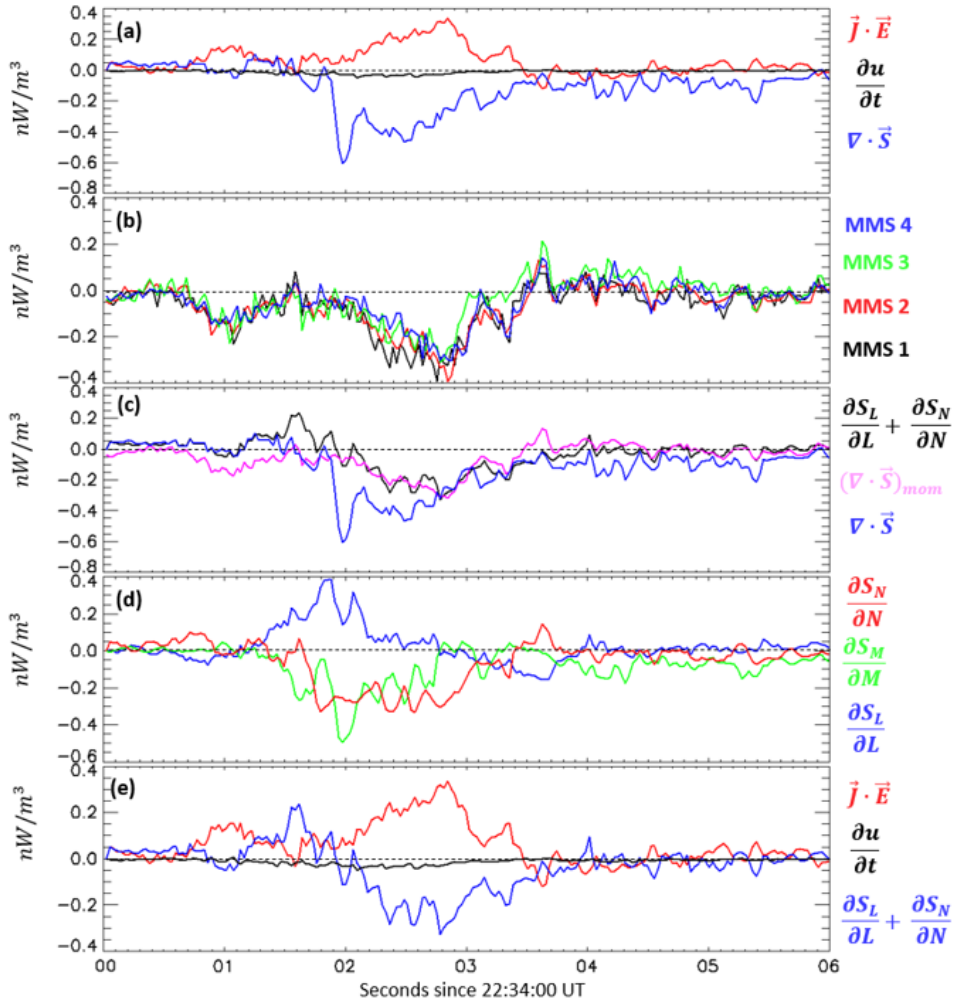

Figure 2. (a) Initial determination of Poynting's theorem terms, (b) $(\nabla \cdot \vec{S})_{mom}$ for each spacecraft, (c) Comparison of all $\nabla \cdot \vec{S}$ calculations, (d) Contributions to $\nabla \cdot \vec{S}$ along LMN axes, (e) Poynting's theorem terms assuming quasi-2D reconnection

160

3.3 Reconstruction of $\nabla \cdot \vec{S}$

Here we show the results of a new method of calculating $\nabla \cdot \vec{S}$ that utilizes a novel 2nd order 3D field reconstruction technique (Torbert et al., 2020). In short, the method solves for a quadratic model of the electric and magnetic fields within the MMS tetrahedron that is both consistent with the measurements at each spacecraft and solves Maxwell's equations everywhere. In figure 3 we compare the reconstructed $\nabla \cdot \vec{S}$ to the other methods and approximations discussed previously.

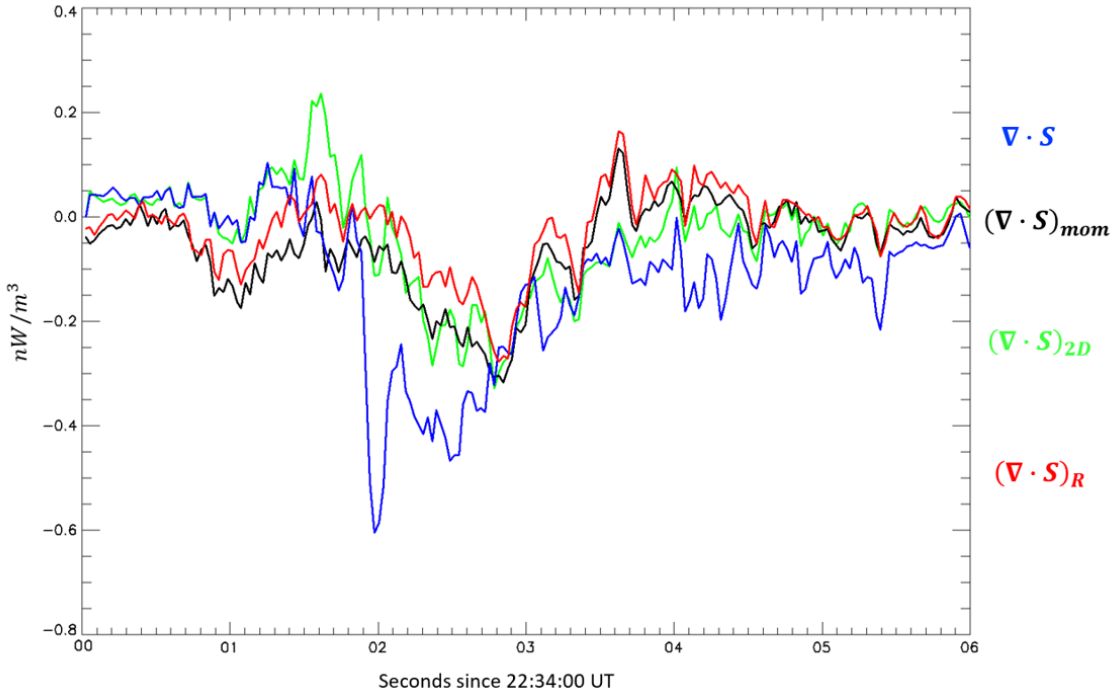

Figure 3. Comparison of the reconstruction $(\nabla \cdot \vec{S})_R$ to the other methods of approximation: Linear gradient method $(\nabla \cdot \vec{S})$, 'Moments' $(\nabla \cdot \vec{S})_{mom}$, and quasi-2D assumption $(\nabla \cdot \vec{S})_{2D}$

The reconstruction result is similar to the quasi-2D result and $(\nabla \cdot \vec{S})_{mom}$ in the central EDR. There is a discrepancy of between roughly $0.1-0.3 nW/m^3$ between the reconstruction and the original $\nabla \cdot \vec{S}$ calculation. The sign of the discrepancy is not consistent over the event; the reconstruction being larger than the original term from 22:34:02-03 UT but smaller beforehand. The larger discrepancy after 22:34:02 UT may be due to very small field magnitudes making it difficult to obtain accurate spatial derivatives. Spatial derivatives may be comparable to the noise in the data when field magnitudes

are close to zero. In fact, the component of $\nabla \cdot \vec{S}$ that contributes most to the discrepancy is $\frac{\partial S_M}{\partial M}$ (figure 1d). Fluctuations in the out-of-plane component of Poynting flux $S_M \approx E_N \times B_L$ may skew the calculation of the gradient after 22:34:02 UT as the E_N and B_L components approach zero, leading to an artificially large $\frac{\partial S_M}{\partial M}$ and $\nabla \cdot \vec{S}$.

4 Simulation Comparisons and Time-Dependence

In the case of the July 11th 2017 EDR, there is a relatively steady balance of electromagnetic energy flux to support the energy transfer rate $\vec{J} \cdot \vec{E}$, therefore there is very little time evolution of the electromagnetic energy density in the current sheet. Whether or not this is indicative of steady-state reconnection is an important question to consider. We investigate this by evaluating each term in equation 1 in the EDR as described previously in section 2. These results are shown in figure 4, along with the out-of-plane component of the electric field. As the out of plane reconnection electric field grows, the elec-

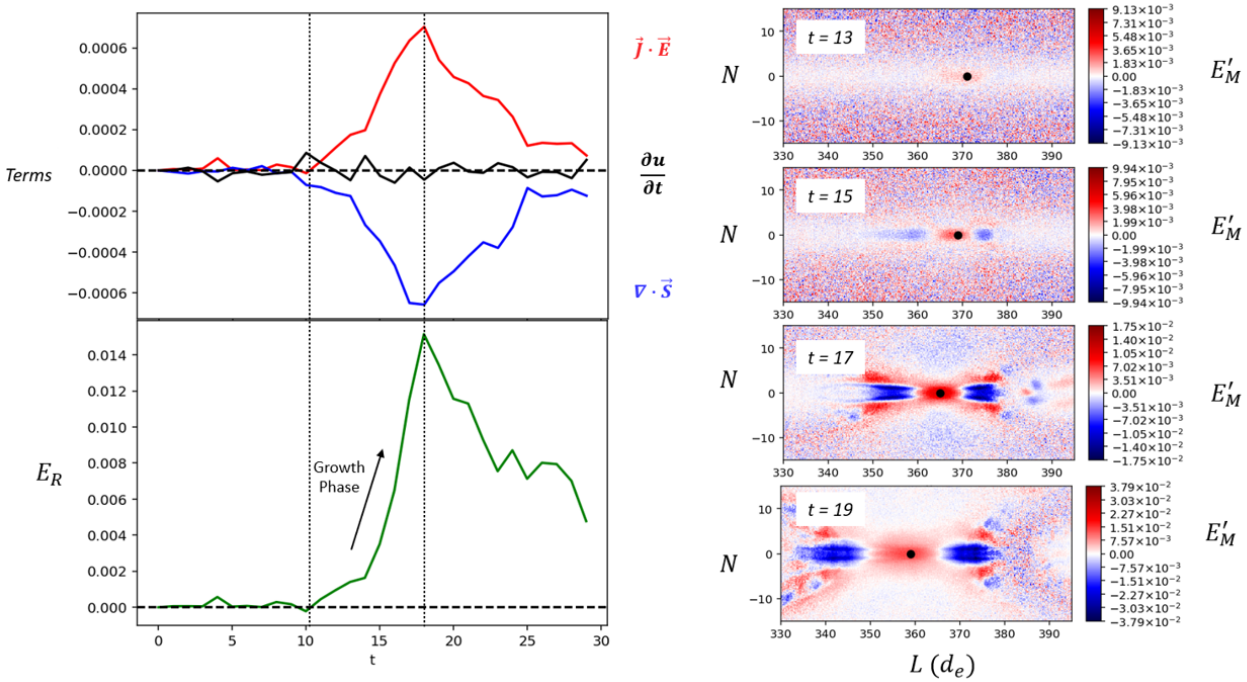

Figure 4. Left: Poynting's theorem terms (top) and the out-of-plane reconnection electric field E_R (bottom) in the EDR during reconnection growth. Right: E'_M at multiple timesteps within the growth phase, including a black dot indicating where each of the terms were evaluated.

tromagnetic field energy transfer rate grows until reconnection stablizes. The balance

between $\boldsymbol{\nabla}\cdot\vec{S}$ and $\vec{J}\cdot\vec{E}$ over the entire evolution suggests that, even in the early growth of reconnection, the electromagnetic energy flowing into the diffusion region will balance the plasma energization such that the electromagnetic energy density is constant. The central EDR in the growth phase as well as the steady state phase of reconnection remains in approximate energy balance such that the electromagnetic energy density remains roughly constant. However, beyond the border of the central EDR Poynting's theorem exhibited significant contributions from all three terms, including $\frac{\partial u}{\partial t}$.

These results suggest that the current sheet in the central EDR is characterized by a region of constant electromagnetic energy density, while the outer EDR and exhaust regions are characterized by stronger time-dependent fluctuations and turbulent structures. The EDR can exhibit a time-independent energy balance, even as it evolves on ion timescales.

The July 11th EDR and the simulation used in this study are examples of 2D reconnection. Large turbulent structures, asymmetries, guide fields, and other 3D effcts may influence these dynamics and are worth further exploration.

5 Conclusion

We have presented a determination of Poynting's theorem by MMS during an encounter with an EDR in the magnetotail. The path of MMS was largely along the path of the flow reversal, providing a view of a single x-line at multiple locations along the neutral sheet. The results suggest that the field to plasma energy conversion rate in the EDR is roughly balanced by the net electromagnetic energy flowing into the region, keeping the electromagnetic energy density in the EDR roughly constant. We have also presented results from a 2D PIC simulation, testing whether or not the balance of Poynting's theorem says anything about reconnection being in a particular stage of evolution. The simulation results suggest that, at least in an idealized two dimensional case, the central EDR always exhibits a roughly constant electromagnetic energy density, even during ion-timescale evolution of the x-line. This result has important implications for x-lines in general. If the central EDR is characterized by this time-independence, while the edges of the EDR exhibit more significant time-dependence in equation 1, then the boundaries of the EDR along the outflow direction are defined by deviations in $\frac{\partial u}{\partial t}$. It is important to consider how these potential boundary conditions could be used to predict

the geometry of x-lines under a given set set of initial conditions, such as plasma density and the strength of the magnetic field, among others.

Acknowledgments

The MMS data used in this study were taken from the Science Data Center (SDC) based at LASP in Boulder, CO (https://lasp.colorado.edu/mms/sdc/). The calibrated L3 electric field data has been made public as well (http://mmspubdata.sr.unh.edu/Dominic-Payne/). The simulation used in this study was run on the CRAY supercomputer Trillian at the University of New Hampshire in Durham, NH. The simulation data and the second order reconstruction data is currently being archived in a Zenodo repository (DOI 10.5281/zenodo.3932337). This work would not be possible without the MMS data and the teams responsible for the development, maintenance, and calibration of the instruments. This work also depends on those who maintain and operate Trillian at UNH. Funding for this work comes from NASA via grants NNG04EB9C and NNX13AK31G as well as NSF funding via NSF-1460190. I would also like to thank everyone in our research group, whose assistance and advice was invaluable.

References

Birn, J., & Hesse, M. (2005). Energy release and conversion by reconnection in the magnetotail. In *Annales geophysicae* (Vol. 23, pp. 3365–3373).

Birn, J., & Hesse, M. (2010). Energy release and transfer in guide field reconnection. *Physics of Plasmas*, *17*(1), 012109.

Burch, J., & Phan, T. (2016). Magnetic reconnection at the dayside magnetopause: Advances with mms. *Geophysical Research Letters*, *43*(16), 8327–8338.

Egedal, J., Olson, J., Greess, S., Millet-Ayala, A., Myers, R., & Forest, C. (2019). Collisionless reconnection with electron pressure anisotropy explored in the terrestrial reconnection experiment (trex). *AGUFM*, *2019*, SM23B–07.

Ergun, R., Tucker, S., Westfall, J., Goodrich, K., Malaspina, D., Summers, D., … others (2016). The axial double probe and fields signal processing for the mms mission. *Space Science Reviews*, *199*(1-4), 167–188.

Frey, H., Phan, T., Fuselier, S., & Mende, S. (2003). Continuous magnetic reconnection at earth's magnetopause. *Nature*, *426*(6966), 533–537.

Genestreti, Nakamura, T., Nakamura, R., Denton, R., Torbert, R., Burch, J., … oth-

ers (2018). How accurately can we measure the reconnection rate em for the mms diffusion region event of 11 july 2017? *Journal of Geophysical Research: Space Physics*, *123*(11), 9130–9149.

Genestreti, K. J., Cassak, P. A., Varsani, A., Burch, J. L., Nakamura, R., & Wang, S. (2018). Assessing the time dependence of reconnection with poynting's theorem: Mms observations. *Geophysical Research Letters*, *45*(7), 2886–2892.

Germaschewski, K., Fox, W., Abbott, S., Ahmadi, N., Maynard, K., Wang, L., … Bhattacharjee, A. (2016). The plasma simulation code: A modern particle-in-cell code with patch-based load-balancing. *Journal of Computational Physics*, *318*, 305–326.

Lindqvist, P.-A., Olsson, G., Torbert, R., King, B., Granoff, M., Rau, D., … others (2016). The spin-plane double probe electric field instrument for mms. *Space Science Reviews*, *199*(1-4), 137–165.

Nakamura, R., Genestreti, K. J., Nakamura, T., Baumjohann, W., Varsani, A., Nagai, T., … others (2019). Structure of the current sheet in the 11 july 2017 electron diffusion region event. *Journal of Geophysical Research: Space Physics*, *124*(2), 1173–1186.

Nakamura, T., Genestreti, K., Liu, Y.-H., Nakamura, R., Teh, W.-L., Hasegawa, H., … others (2018). Measurement of the magnetic reconnection rate in the earth's magnetotail. *Journal of Geophysical Research: Space Physics*, *123*(11), 9150–9168.

Paschmann, G., & Schwartz, S. (2000). Issi book on analysis methods for multi-spacecraft data. In *Cluster-ii workshop multiscale/multipoint plasma measurements* (Vol. 449, p. 99).

Pollock, C., Moore, T., Jacques, A., Burch, J., Gliese, U., Saito, Y., … others (2016). Fast plasma investigation for magnetospheric multiscale. *Space Science Reviews*, *199*(1-4), 331–406.

Russell, C., Anderson, B., Baumjohann, W., Bromund, K., Dearborn, D., Fischer, D., … others (2016). The magnetospheric multiscale magnetometers. *Space Science Reviews*, *199*(1-4), 189–256.

Torbert, R., Burch, J., Phan, T., Hesse, M., Argall, M., Shuster, J., … others (2018). Electron-scale dynamics of the diffusion region during symmetric magnetic reconnection in space. *Science*, *362*(6421), 1391–1395.

Torbert, R., Dors, I., Argall, M., Genestreti, K., Burch, J., Farrugia, C., … Strangeway, R. (2020). A new method of 3-d magnetic field reconstruction. *Geophysical Research Letters*, *47*(3), e2019GL085542.

Zenitani, S., Hesse, M., Klimas, A., & Kuznetsova, M. (2011). New measure of the dissipation region in collisionless magnetic reconnection. *Physical review letters*, *106*(19), 195003.